Applied Physics Letters

Investigation of trapping effects in Schottky lightly doped P-GaN gate stack under γ-ray irradiation

Cite as: Appl. Phys. Lett. **121**, 143501 (2022); https://doi.org/10.1063/5.0094090
Submitted: 01 April 2022 • Accepted: 13 September 2022 • Published Online: 04 October 2022

Peng Wang, Yizhou Jiang, Yitian Gu, et al.

View Online Export Citation CrossMark

ARTICLES YOU MAY BE INTERESTED IN

Alkaline plasma-activated water (PAW) as an innovative therapeutic avenue for cancer treatment
Applied Physics Letters **121**, 144101 (2022); https://doi.org/10.1063/5.0107906

High-performance electron mobility and photoabsorption in Bi_2O_2Se nanoribbons
Applied Physics Letters **121**, 141902 (2022); https://doi.org/10.1063/5.0111109

UV-A to UV-B electroluminescence of core-shell GaN/AlGaN wire heterostructures
Applied Physics Letters **121**, 131102 (2022); https://doi.org/10.1063/5.0101591

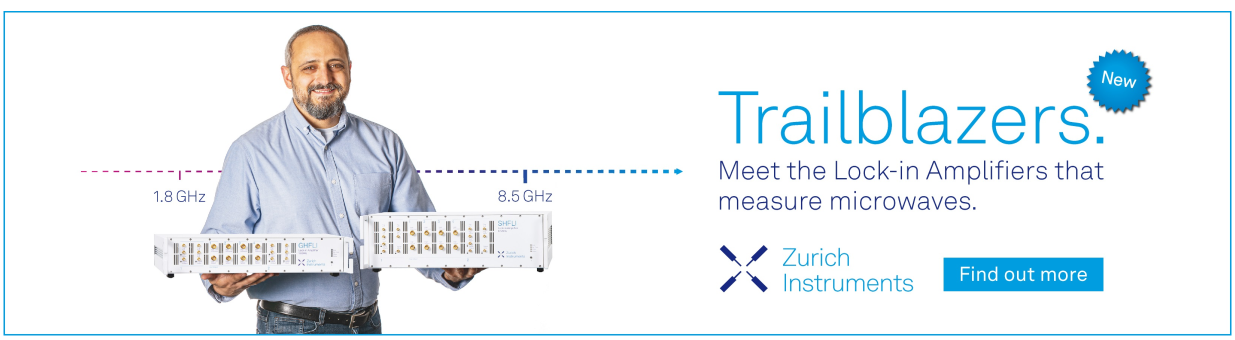

© 2022 Author(s).

Applied Physics Letters ARTICLE scitation.org/journal/apl

Investigation of trapping effects in Schottky lightly doped P-GaN gate stack under γ-ray irradiation

Cite as: Appl. Phys. Lett. **121**, 143501 (2022); doi: 10.1063/5.0094090
Submitted: 1 April 2022 · Accepted: 13 September 2022 ·
Published Online: 4 October 2022

View Online Export Citation CrossMark

Peng Wang,[1] Yizhou Jiang,[1] Yitian Gu,[2] Menglin Huang,[1] Wei Huang,[1,a)] Shiyou Chen,[1,a)] Zhiqiang Xiao,[1,3,a)] Xinbo Zou,[2] Yiwu Qiu,[3] Xinjie Zhou,[3] Jianjun Zhou,[4] and David Wei Zhang[1]

AFFILIATIONS

[1]State Key Laboratory of ASIC and System, Shanghai Institute of Intelligent Electronics & Systems, School of Microelectronics, Fudan University, Shanghai 200433, China
[2]School of Information Science and Technology (SIST), ShanghaiTech University, Shanghai, China and Shanghai Institute of Microsystem and Information Technology, Chinese Academy of Sciences, Shanghai, China
[3]Wuxi Microelectronics Scientific and Research Center, Wuxi 214035, China
[4]Nanjing Electronic Device Institute, Nanjing 210016, China

[a)]Authors to whom correspondence should be addressed: eehuangw@fudan.edu.cn; chensy@fudan.edu.cn; and 2962504225@qq.com

ABSTRACT

In this Letter, trapping effects of a Schottky lightly Mg-doped p-GaN gate stack for low-power applications have been investigated, and further analysis focusing on AlGaN/GaN interface traps under γ-ray irradiation has been carried out. A negligible shift in the flatband voltage with γ-ray irradiation dose up to 800 krad indicates the superior radiation tolerance of the p-GaN gate structure. The difference between capacitance dispersion at the measurement frequency below and above 500 kHz is observed, which is attributed to trapping effects in different locations with varying gate voltage. Moreover, the frequency-dependent conductance method is put forward to assess the effects of different doses of γ-ray irradiation on the AlGaN/GaN interface traps. Based on that method, aside from the shallow trap states [the trap activation energy (E_T) is about 0.334–0.338 eV] previously found in the traditional normally on high electron mobility transistor (HEMT), another type of deeper trap states at the AlGaN/GaN interface (E_T is about 0.467–0.485 eV) is detected. It is observed that the E_T of shallow trap states distributes at a deeper and broader range as the irradiation dose increases. Additionally, the trap density decreased after 600 krad doses irradiation but increased after 800 krad doses irradiation for both deep and shallow E_T. Transmission electron microscopy and atomic force microscopy are used to demonstrate the smooth AlGaN/GaN interface morphology, which will not be greatly damaged after 800 krad doses of γ-ray irradiation. This work can provide a further understanding of radiation tolerance and trapping effects of p-GaN gate HEMTs for low-voltage applications.

Published under an exclusive license by AIP Publishing. https://doi.org/10.1063/5.0094090

Semiconductor devices would be irradiated by many electromagnetic and particle radiations in harsh aerospace environments, including heavy ions, γ ray, x ray, and protons.[1,2] Owing to the wide bandgap of GaN, GaN-based power devices exhibit excellent irradiation resistance, which promotes them to be promising transistors in space applications.[1,3] Introducing a p-GaN epilayer is a high-stability and low-cost implementation method to realize normally off operation for power high electron mobility transistors (HEMTs).[4]

γ-Ray irradiation's influences on GaN-based HEMTs were widely investigated by several works. Some researchers have reported the improved electrical performance of AlGaN/GaN normally on HEMTs following γ-ray irradiation, which is attributed to the reduction/rearrangement of crystal defects, the increase in the carrier concentration of the 2DEG channel, the creation of the nitrogen vacancies, or the improvement in the 2DEG mobility.[5–10] In contrast, other studies reported that degradation is observed in the performance of normally on HEMTs after γ-ray irradiation.[11] As for the studies about normally off HEMTs, Lidow *et al.*[12] and Gerardin[13] reported that little change is seen in electrical characteristics when the devices are subjected to a total γ-ray dose of 500 krad and 1.08 Mrad, respectively. Tang *et al.*[14] found that the normally off HEMTs showed improved electrical properties after γ-ray irradiation, including increased drain current and decreased gate current. The improvement is explained by the creation of nitrogen vacancy offering the electrons in the 2DEG channel and

Published under an exclusive license by AIP Publishing

the annealing of the interfacial trap centers.[14] The detailed trapping mechanism of the p-GaN gate stack under γ-ray irradiation should be further investigated. On the other hand, AlGaN/GaN interface traps have a considerable impact on the mobility of carriers in the 2DEG channel through Coulomb scattering, thereby degrading device electrical performance such as the sheet resistance and channel mobility.[15,16] However, quantitative studies on AlGaN/GaN interface traps in p-GaN gate HEMTs following γ-ray irradiation are seldom reported.

For high-efficiency power conversion in space applications, the GaN-based normally off devices with low V_{th} or low on-resistance are indispensable.[17] It is known that the V_{th} of the p-GaN gate HEMTs is highly dependent on the activated Mg concentration in the p-GaN layer.[17–19] The quality of the epitaxial layer and the doping level highly affect the generation of defects.[7] Therefore, studying the shift of electrical characteristics including V_{th} due to γ-ray irradiation in lightly doped p-GaN gate HEMTs is essential.

In this Letter, the low-V_{th} Schottky p-GaN gate stack for low on-resistance and high-frequency applications is fabricated by lightly doping Mg in the p-GaN layer. The V_{th} stability of these devices is studied by comparing unirradiated and irradiated ones. Moreover, the frequency-dependent conductance technique is utilized to quantitatively characterize the AlGaN/GaN interface traps in these devices under γ-ray irradiation. Two types of AlGaN/GaN interface traps have been observed, and parameter variations of them after different doses of γ-ray irradiation have been discussed.

The inset of Fig. 1 shows the schematic cross section of the tested p-GaN gate stack circular capacitor. The epitaxial structure consists of an AlN layer, a GaN buffer layer, a 15 nm $Al_{0.2}Ga_{0.8}N$ barrier layer, and a 70 nm lightly Mg-doped p-GaN cap layer. Note that the lightly doping concentration of Mg is about $2 \times 10^{17}\,cm^{-3}$. The Schottky metal, which enables the gate to reduce leakage, was deposited on the p-GaN layer at the start of the process. Then a circular gate region with a radius of 100 μm that contains the p-GaN layer and Schottky metal stack was fabricated by etching. After finishing device isolation, the Ohmic contact, which is designed as a ring surrounding the gate with a spacing of 10 μm, was formed. The C–V measurement of multiple unirradiated devices was carried out by using an Agilent B1500A semiconductor analyzer, and the test results of them are nearly consistent. Two devices were irradiated with different γ-ray (^{60}Co) doses, i.e., 600 and 800 krad at a dose rate of 100 rad/s. Irradiation was conducted at room temperature, and the device's terminals are grounded. Post-irradiation devices were measured ~48 h after irradiation by the same analyzer at room temperature.

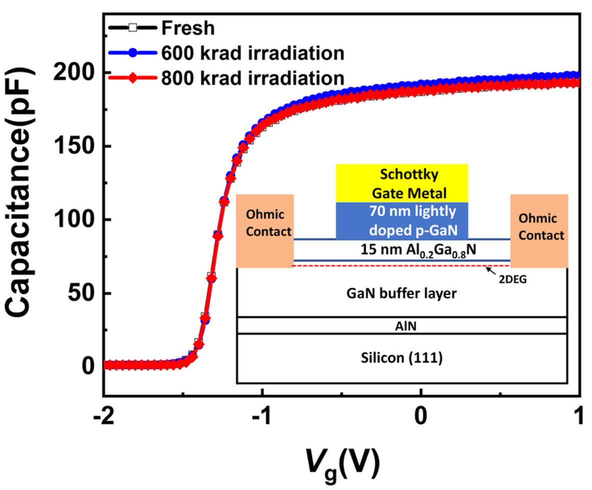

FIG. 1. Dependence of capacitance on the gate voltage at 100 kHz before and after different γ-ray irradiation doses. The inset shows the schematic cross section of the measured p-GaN gate stack circular capacitor structure.

The C–V measurement was applied to samples as f_m (measurement frequency) varies from 300 Hz to 5 MHz. Figure 1 shows C–V measurement curves before and after doses of 600 and 800 krad irradiation when $f_m = 100$ kHz. The shift in the flatband voltage (ΔV_{FB}) is negligible even if the irradiation dose is increased to 800 krad, which is consistent with the literature.[12] It is concluded that the devices feature outstanding γ-ray irradiation resistance.

Figures 2(a) and 2(b) depict the C–V dependence of the fresh sample at f_m ranging from 300 Hz to 500 kHz and 500 kHz to 5 MHz, respectively. The C–V curves of the fresh sample can be divided into three regions: (1) region I ($V_g < -1.5$ V) represents the region in which the 2DEG channel has been fully depleted. (2) Region II ($-1.5\,V < V_g < -0.5$ V) features a typical turn-off to turn-on transition where the energy band at the AlGaN/GaN heterostructure is gradually pulled down. (3) Region III ($V_g > -0.5$ V) corresponds to the case that the 2DEG channel is in the deep accumulation region. A low concentration of Mg leads to the p-GaN layer being completely depleted in region III.[18] Thus, C–V curves in region III do not display a downward trend. Figure 2(a) and its inset show that capacitance dispersion only appears in region II when $f_m < 500$ kHz. While Fig. 2(b) shows that when $f_m > 500$ kHz, the capacitance dispersion highly depends on the gate voltage and gets more significant at region III. To understand the different capacitance–dispersion behaviors, the dependence of capacitance on f_m at $V_g = -1.3$ and 0 V is shown in Fig. 2(c). Due to trapping effects, (1) when $V_g = -1.3$ V, the capacitance drops with the increase in f_m when $f_m > 50$ kHz, and (2) when $V_g = 0$ V, the capacitance dispersion only occurs when 500 kHz $< f_m <$ 3 MHz.

The different behaviors of capacitance dispersion between $f_m < 500$ kHz and $f_m > 500$ kHz are attributed to traps at the p-GaN/GaN interface failing to respond to ac perturbation of V_g at high f_m. The schematics of interface trapping behaviors at $V_g = -1.3$ V (in region II) and $V_g = 0$ V (in region III) are shown in Fig. 2(d). They depict that there are two types of interface traps that affect the admittance: (I) one type is the hole-traps at the p-GaN/AlGaN interface, and (II) another type is the electron-traps at the AlGaN/GaN interface. It is known that energy levels of the trap states located at the Fermi level can respond to ac signals when ac f_m is lower than $1/(2\pi \times \tau_e)$ (τ_e is the time constant for electron emission of interface traps) and the trapping and de-trapping processes of them contribute to additional capacitance (C_t) and energy loss.[16] When $V_g = -1.3$ V, both types of trap states can contribute additional capacitance as long as f_m is matched. However, when $V_g = 0$ V, the 2DEG channel turns into the accumulation region; as a result, the Fermi level is higher than all of the energy levels of the trap states at the AlGaN/GaN interface. In the latter case, no matter what f_m is, the AlGaN/GaN interface traps can hardly be detected via this method. Therefore, the hole-traps at the p-GaN/GaN interface are responsible for capacitance dispersion in region III. Due to the capacitance dispersion caused by p-GaN/GaN interface traps only occurring when $f_m > 500$ kHz, it is reasonable to

Published under an exclusive license by AIP Publishing

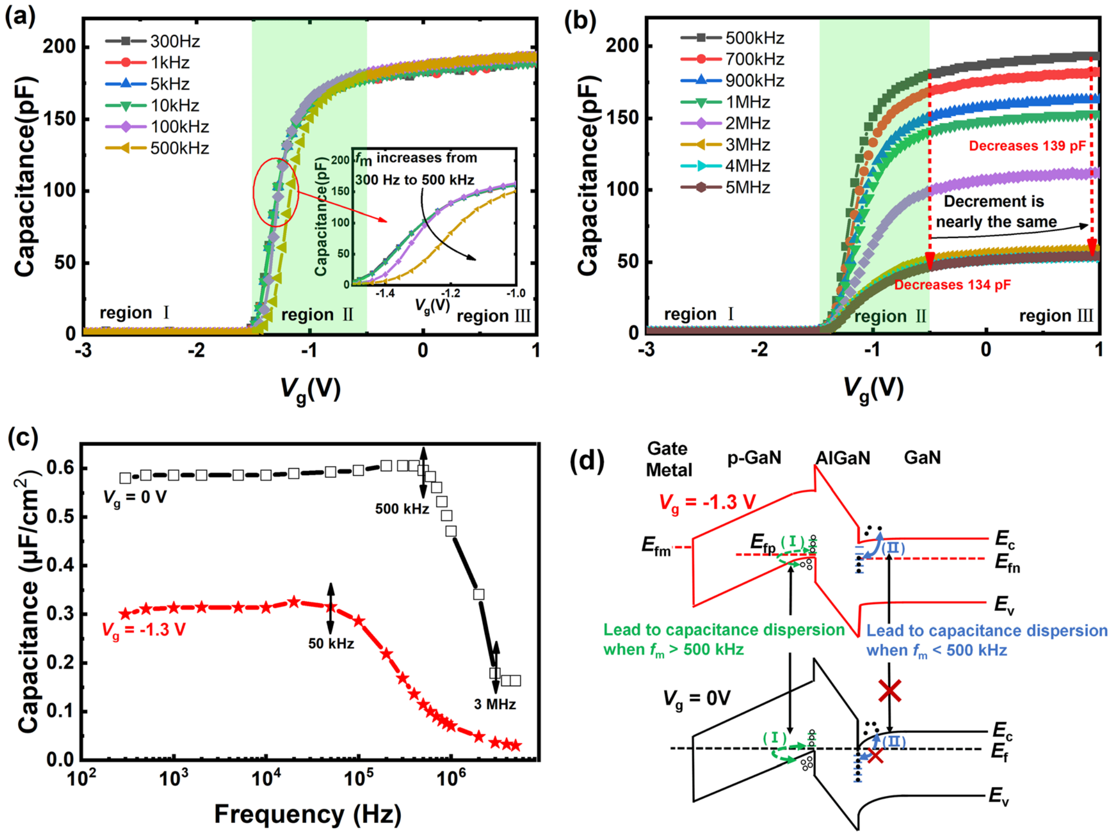

FIG. 2. C–V characteristics of the fresh p-GaN gate circular Schottky barrier diode sample under f_m at (a) 300 Hz–500 kHz and (b) 500 kHz–5 MHz. The inset amplifies the C–V curves from -1.5 to -1 V. (c) Dependence of capacitance on f_m at $V_g = -1.3$ and 0 V. (d) Band diagram and interface trapping behaviors of the p-GaN gate stack at $V_g = -1.3$ and 0 V.

deduce that the capacitance dispersion in region II when $f_m < 500$ kHz is only caused by electron-traps at the AlGaN/GaN interface. Typically, bulk traps located at the GaN or AlGaN layer have a time constant longer than 1 ms.[16] Because the capacitance of the studied samples does not decrease until f_m is higher than 50 kHz as shown in Fig. 2(c), neglecting bulk traps in this work is reasonable.

It is observed in Fig. 2(b) that the decrement for capacitance is nearly independent of V_g in region III (from $\Delta C = -134$ pF to $\Delta C = -139$ pF). This is due to the high polarized charge at the p-GaN/AlGaN interface, and the valence band is only slightly pulled down when V_g increases.[20] The phenomenon also provides a proof for the deduction that trapping effects happened at the p-GaN/AlGaN interface is the dominant reason for capacitance dispersion in region III.

On the other hand, frequency-dependent conductance measurement is utilized to investigate the density and distribution of the AlGaN/GaN interface states by improving the model of a p-GaN gate stack capacitor. Normally, the capacitor consists of two back-to-back diodes, namely, a p-GaN/metal Schottky diode (D_{Sch}) and a p-GaN/AlGaN/GaN diode (D_{pin}).[16] Aside from that, considering C_{GaN} and trap states induced admittance, i.e., C_{tn}, G_{tn} (AlGaN/GaN interface traps induced capacitance and conductance) and C_{tp}, G_{tp} (p-GaN/AlGaN interface traps induced capacitance and conductance), the optimized equivalent circuit can be modeled as the inset (i). The inset (ii) shows the simplified circuit to extract parameters of AlGaN/GaN interface traps, where the accumulation capacitance, C_{total}, represents the total of serially connected AlGaN barrier capacitance (C_{AlGaN}) and p-GaN/metal Schottky capacitance (C_{Sch}), and note that the contributions of G_{tp} and C_{tp} have already been considered when defining C_{total}.

The parallel conductance G_p/ω can be obtained by the measured capacitance (C_m) and conductance (G_m) through the following relation:[16,21]

$$\frac{G_p}{\omega} = \frac{\omega G_m C_{total}^2}{G_m^2 + \omega^2 (C_{total} - C_m)^2}. \tag{1}$$

The G_p/ω, which is calculated through Eq. (1), vs ω at selected gate bias for fresh and irradiated samples is shown in Fig. 3. Note that the experimentally measured G_p/ω has two peaks for all tested samples. Assuming the interface state comprises a single energy level, the relationship between G_p/ω and ω can be expressed according to the following equation:[16,21]

$$\frac{G_p}{\omega} = \frac{q\omega\tau_{ts} D_{ts}}{1 + (\omega\tau_{ts})^2} + \frac{q\omega\tau_{tf} D_{tf}}{1 + (\omega\tau_{tf})^2}, \tag{2}$$

where D_{ts} (D_{tf}) is the slow (fast) trap states density at the AlGaN/GaN interface and τ_{ts} (τ_{tf}) is the slow (fast) trap states time constant.

Published under an exclusive license by AIP Publishing

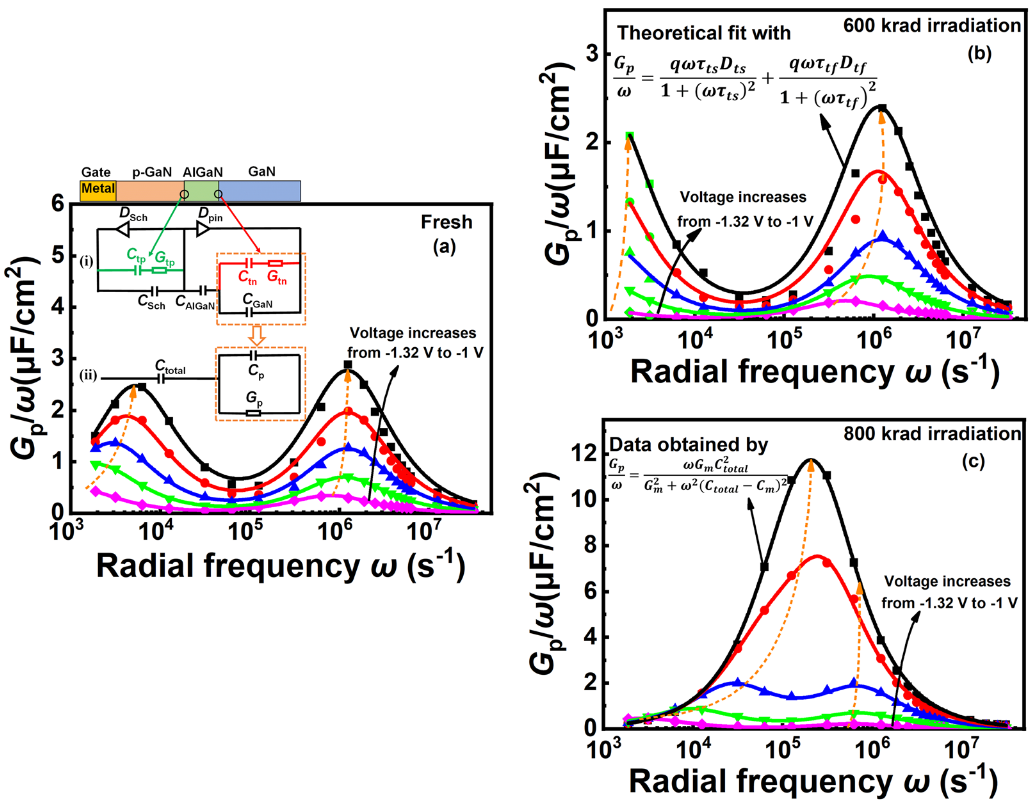

FIG. 3. G_p/ω as a function of ω at selected gate bias (a) before, (b) after 600 krad, and (c) after 800 krad irradiation. The inset in (a) shows the schematic of the p-GaN gate stack and equivalent circuit model: (i) with consideration of p-GaN/AlGaN and AlGaN/GaN interface traps, (ii) converted to a simplified circuit to study AlGaN/GaN interface traps.

Based on Eq. (2), the G_p/ω vs ω is fitted. It is observed that the fitting lines are in great agreement with experimental data, regardless of whether the device has been exposed to γ-ray irradiation. It can be obtained that the time constants and trap densities for the fast and slow trap states in the fresh sample are τ_{tf} = 0.55–0.62 μs, D_{tf} = 2.0–7.5 $\times 10^{13}$ cm^{-2}eV^{-1} and τ_{ts} = 90–183 μs, D_{ts} = 2.9–7.3 $\times 10^{13}$ cm^{-2}eV^{-1}, respectively. For irradiated samples, the time constants have been significantly changed, since the ω corresponding to the maximum G_p/ω shows an obvious shift.

In addition, the parameters, including trap density D_t and time constant τ_t, are extracted in Fig. 4. Figure 4(a) shows the τ_t of the fast and slow trap state vs gate bias. Nearly exponential τ_t–V_g dependence is obtained for the fresh sample. However, τ_t of the fast trap of the 800 krad irradiated sample exhibits a deviation from this relationship since the two peaks of the fitting line in Fig. 3(c) are too close to be clearly distinguished between their respective contributions. The trap activation energy E_T is determined from τ_t by the following equation:[22]

$$\tau_t = \frac{1}{\upsilon_{th}\sigma_n N_c}\exp\left(\frac{E_T}{kT}\right), \tag{3}$$

where υ_{th} is the average thermal velocity, σ_n is the electron capture cross section, and N_c represents the density of states in the GaN conduction band. By assigning $T = 300$ K, υ_{th} = 2.6×10^7 cm/s, σ_n = 1×10^{-14} cm^{-2}, and N_c = 2.7×10^{18} cm^{-3}, the D_t as a function of E_T is shown in Fig. 4(b).[22] Note that, according to Eq. (3), the larger τ_t implies a deeper energy level. It is observed that shallow and deep energy levels display different behaviors facing irradiation; thereby, analysis of them will be divided into the next two parts:

1. For traps with shallow energy levels, the E_T range for the fresh sample is 0.334–0.338 eV, which is generally consistent with 0.32–0.34 eV detected from the traditional normally on HEMT.[23] The status of these original defects is probably oxygen-related.[23,24] The location of shallow energy levels is 0.344–0.364 eV for the 600 krad irradiated sample and 0.362–0.386 eV for the 800 krad irradiated sample, which indicates that shallow energy levels gradually deepen and the distribution range of them expands with an increase in the irradiation dose. Deeper trap states newly introduced by irradiation have a more harmful impact on high-frequency applications since the electrons trapped by deep energy levels cannot escape easily. Additionally, it is observed that maximal D_{tf} increases to 3.1 $\times$ 10^{14} cm^{-2} eV^{-1} after 800 krad irradiation. The new deeper trap states induced at the AlGaN/GaN interface by γ-ray irradiation will trap more electrons in the 2DEG channel and form negatively charged centers, which will reduce the mobility of electrons through Coulomb scattering. It can be concluded that high dose γ-ray irradiation may degrade the performance of transistors by increasing the amounts and depth of shallow trap states in the AlGaN/GaN interface.

Published under an exclusive license by AIP Publishing

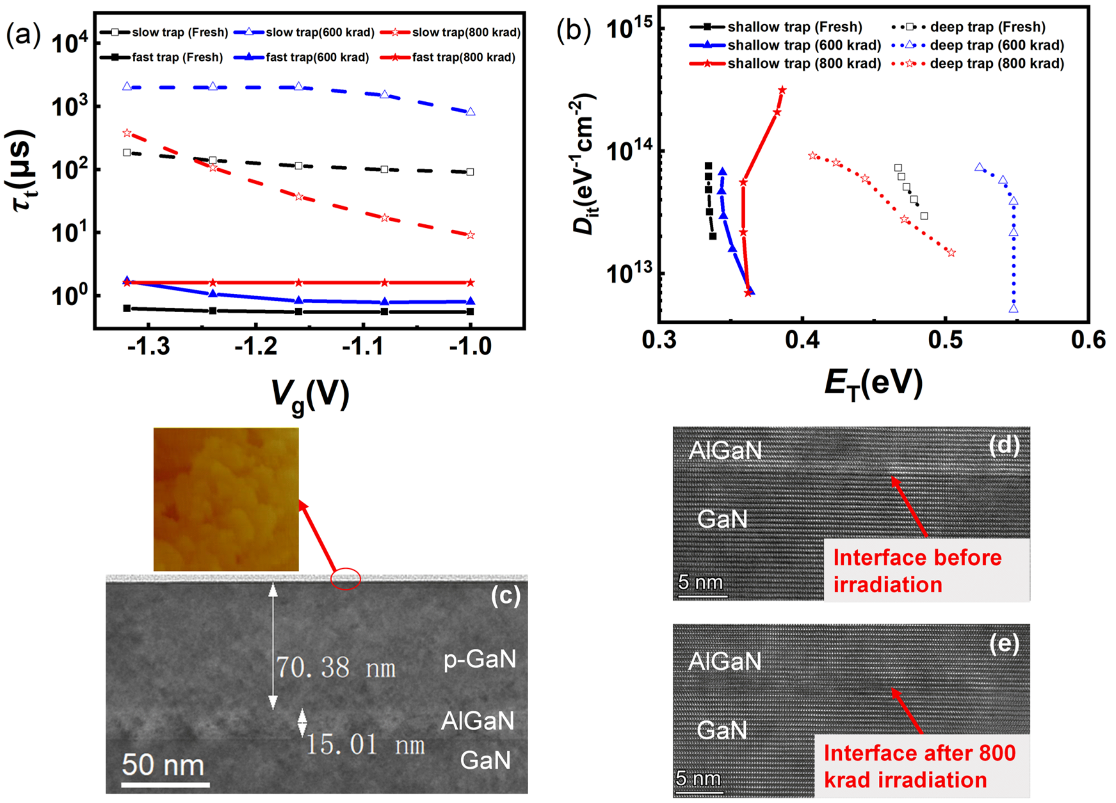

FIG. 4. (a) Voltage dependence of trap time constant and (b) trap state density as a function of the energy level in the AlGaN/GaN interface before and after irradiation. (c) Cross-sectional TEM image of the p-GaN/AlGaN/GaN epitaxial structure without gate metal deposition. The inset shows the atomic force microscopy (AFM) image of surface morphology of the epitaxial structure with $5 \times 5\,\mu m^2$ scan area. TEM images of the AlGaN/GaN interface for (d) fresh and (e) irradiated (800 krad doses) devices.

2. For traps with deep energy levels, the E_T range for the fresh sample is 0.467–0.485 eV, and a trap at this energy level in the AlGaN/GaN interface can be found in the previous studies.[6,15] After irradiation, the deep energy levels deepen to 0.524–0.548 eV for a 600 krad irradiated sample but shallow to 0.407–0.504 eV for an 800 krad irradiated sample. Similar to the shallow energy levels, the distribution range of the deep energy levels gradually expands as the irradiation dose increases.

It is also noted that γ-ray irradiation in HEMT structures can lead to the creation of additional defects or the compensation and structural ordering of native defects.[10] The complex effects caused by γ-ray irradiation make their impact on the performance of different devices very greatly. Figure 4(b) shows that the trap density slightly decreases following 600 krad doses irradiation but dramatically increases after 800 krad doses irradiation. Possible reasons causing this modification are the combined effect of the introduction of new defects and the annealing effect on intrinsic defects.[25,26]

To verify the AlGaN/GaN interface quality for the devices, transmission electron microscopy (TEM) and atomic force microscopy (AFM) analysis are conducted for the fresh and irradiated (800 krad doses) samples. Figure 4(c) shows the TEM image of the pristine epitaxial structure, and the inset shows the AFM image with a $5 \times 5\,\mu m^2$ scan area, which is taken from the surface of the p-GaN layer. It is clearly shown from the AFM image smooth surface morphology of epitaxial layers. The surface roughness in the root mean square (rms) is approximately 0.37 nm. Figures 4(d) and 4(e) show TEM images of the AlGaN/GaN interface for fresh and 800 krad irradiated samples, respectively. The well AlGaN/GaN interface quality can be observed from the images. The result that the calculated lines in Fig. 3 well fit the experimental data is mainly due to the good interface quality and the uniform distribution of interface traps. No significant change can be obtained via comparing the AlGaN/GaN interface for fresh and irradiated devices, which indicates that, under this dose of irradiation, the AlGaN/GaN interface morphology will not be greatly damaged.

In summary, the trapping effects of the lightly Mg-doped p-GaN gate stack before and after different γ-ray doses of irradiation have been investigated. The insignificant ΔV_{FB} is obtained, which suggests the superior γ-ray irradiation tolerance of the p-GaN gate stack. The reason for different capacitance dispersion behaviors at low and high measurement frequencies is discussed, it is attributed to the additional capacitance induced by the p-GaN/GaN interface traps which decreases only when $f_m > 500$ kHz, and capacitance dispersion at the 2DEG channel depletion region when $f_m < 500$ kHz is caused by the trapping effects at the AlGaN/GaN interface. Meanwhile, by utilizing the frequency-dependent conductance method, two types of trap states at the AlGaN/GaN interface are obtained. An excellent fitting result is

Published under an exclusive license by AIP Publishing

exhibited to quantitatively study the effects of γ-ray irradiation on the AlGaN/GaN interface traps in the p-GaN gate stack. The distribution ranges of both types of trap states expand, and the energy levels of fast trap states deepen with an increase in the irradiation dose. The trap density decreases under 600 krad and increases under 800 krad due to rearrangement or generation of crystal defects during irradiation. The TEM images of the AlGaN/GaN interface morphology did not change significantly after γ-ray irradiation. The research results are helpful for further understanding γ-ray irradiation on the trapping behavior of p-GaN gate HEMTs.

The process of sample fabrication was conducted at Fudan Nano-fabrication Lab. This work was supported by the National Natural Science Foundation of China (No. 6202780115), the Key Research and Development Program of Guangdong Province (No. 2020B010171002), and the Key Technology Funding of Shanghai (No. 2020-jmrh1-kj55).

AUTHOR DECLARATIONS

Conflict of Interest

The authors have no conflicts to disclose.

Author Contributions

Peng Wang: Data curation (lead); Investigation (lead); Methodology (lead); Software (equal); Writing – original draft (lead); Writing – review & editing (lead). **Xinjie Zhou:** Conceptualization (equal); Funding acquisition (equal); Resources (equal); Supervision (equal). **Jianjun Zhou:** Conceptualization (equal); Funding acquisition (equal); Project administration (equal); Resources (lead); Supervision (equal); Validation (equal); Visualization (equal); Writing – review & editing (equal). **David Wei Zhang:** Funding acquisition (equal); Project administration (equal); Resources (equal). **Yizhou Jiang:** Investigation (equal); Methodology (equal); Software (equal); Validation (equal). **Yitian Gu:** Data curation (equal); Formal analysis (equal); Methodology (equal); Supervision (equal); Validation (equal). **Menglin Huang:** Conceptualization (equal); Data curation (equal); Formal analysis (equal); Software (equal); Validation (equal). **Wei Huang:** Conceptualization (lead); Data curation (equal); Formal analysis (equal); Funding acquisition (lead); Project administration (lead); Resources (lead); Software (equal); Supervision (equal); Writing – original draft (equal); Writing – review & editing (equal). **Shiyou Chen:** Conceptualization (equal); Data curation (equal); Formal analysis (equal); Methodology (equal); Resources (equal); Supervision (equal). **Zhi-Qiang Xiao:** Conceptualization (equal); Funding acquisition (equal); Project administration (equal); Software (equal); Supervision (equal); Validation (equal); Visualization (equal). **Xinbo Zou:** Conceptualization (equal); Formal analysis (equal); Funding acquisition (equal); Software (equal); Supervision (equal); Validation (equal). **Yiwu Qiu:** Conceptualization (equal); Data curation (equal); Formal analysis (equal); Investigation (equal); Methodology (equal); Resources (equal); Validation (equal); Writing – review & editing (equal).

DATA AVAILABILITY

The data that support the findings of this study are available from the corresponding authors upon reasonable request.

REFERENCES

[1] R. Sun, X. Chen, C. Liu, W. Chen, and B. Zhang, Appl. Phys. Lett. **119**, 133503 (2021).
[2] X.-X. Li, J.-X. Chen, W. Huang, Z. Ji, Z.-H. Feng, S.-Z. Wu, Z.-Q. Xiao, and H.-L. Lu, in *IEEE International Symposium on the Physical and Failure Analysis of Integrated Circuits (IPFA)* (IEEE, 2020), pp. 1–4.
[3] J.-L. Zhang, P. Ding, B. Mei, S.-H. Meng, C. Zhang, L.-H. Ma, Z. Jin, Y. Sun, H.-M. Zhang, and Y.-H. Zhong, Appl. Phys. Lett. **120**, 103501 (2022).
[4] A. N. Tallarico, S. Stoffels, P. Magnone, N. Posthuma, E. Sangiorgi, S. Decoutere, and C. Fiegna, IEEE Electron Device Lett. **38**, 99 (2017).
[5] C. Sharma, A. K. Visvkarma, R. Laishram, A. Malik, K. Narang, S. Vinayak, and R. Singh, Semicond. Sci. Technol. **34**, 065024 (2019).
[6] S. Pan, S. Feng, X. Li, X. Zheng, X. Lu, C. Hu, X. He, K. Bai, L. Zhou, and Y. Zhang, Semicond. Sci. Technol. **36**, 095011 (2021).
[7] C. Sharma, R. Singh, D.-S. Chao, and T.-L. Wu, J. Electron. Mater. **49**, 6789 (2020).
[8] A. M. Kurakin, S. A. Vitusevich, S. V. Danylyuk, H. Hardtdegen, N. Klein, Z. Bougrioua, B. A. Danilchenko, R. V. Konakova, and A. E. Belyaev, J. Appl. Phys. **103**, 083707 (2008).
[9] S. A. Vitusevich, A. M. Kurakin, R. V. Konakova, A. E. Belyaev, and N. Klein, Appl. Surf. Sci. **255**, 784 (2008).
[10] C. Sharma, N. Modolo, H.-H. Chen, Y.-Y. Tseng, S.-W. Tang, M. Meneghini, G. Meneghesso, E. Zanoni, R. Singh, and T.-L. Wu, Microelectron. Reliab. **100–101**, 113349 (2019).
[11] C. Schwarz, A. Yadav, M. Shatkhin, E. Flitsiyan, L. Chernyak, V. Kasiyan, L. Liu, Y. Y. Xi, F. Ren, S. J. Pearton, C. F. Lo, J. W. Johnson, and E. Danilova, Appl. Phys. Lett. **102**, 062102 (2013).
[12] A. Lidow, A. Nakata, M. Rearwin, J. Strydom, and A. M. Zafrani, in *IEEE Radiation Effects Data Workshop (REDW)* (IEEE, 2014), pp. 1–7.
[13] S. Gerardin, in *Proceedings of 11th International Conference on Large Scale Applications and Radiation Hardness of Semiconductor Detectors (RD 13)* (Sissa Medialab, Florence, Italy, 2015).
[14] S.-W. Tang, P.-Y. Yao, D.-S. Chao, T.-L. Wu, and H.-M. Hsu, Microelectron. Reliab. **126**, 114425 (2021).
[15] X. Zheng, S. Feng, Y. Zhang, X. He, and Y. Wang, IEEE Trans. Electron Devices **64**, 1498 (2017).
[16] T. Zhu, X.-F. Zheng, J. Wang, M.-S. Wang, K. Chen, X.-H. Wang, M. Du, P.-J. Ma, H. Zhang, L. Lv, Y.-R. Cao, X.-H. Ma, and Y. Hao, IEEE Trans. Nucl. Sci. **68**, 2616 (2021).
[17] G. Greco, F. Iucolano, and F. Roccaforte, Mater. Sci. Semicond. Process. **78**, 96 (2018).
[18] N. Modolo, S.-W. Tang, H.-J. Jiang, C. De Santi, M. Meneghini, and T.-L. Wu, IEEE Trans. Electron Devices **68**, 1489 (2021).
[19] T.-L. Wu, B. Bakeroot, H. Liang, N. Posthuma, S. You, N. Ronchi, S. Stoffels, D. Marcon, and S. Decoutere, IEEE Electron Device Lett. **38**, 1696 (2017).
[20] M. Ťapajna, O. Hilt, E. Bahat-Treidel, J. Würfl, and J. Kuzmík, Appl. Phys. Lett. **107**, 193506 (2015).
[21] K. Zhang, J. Xue, M. Cao, L. Yang, Y. Chen, J. Zhang, X. Ma, and Y. Hao, J. Appl. Phys. **113**, 174503 (2013).
[22] Z. Zhang, G. Yu, X. Zhang, X. Deng, S. Li, Y. Fan, S. Sun, L. Song, S. Tan, D. Wu, W. Li, W. Huang, K. Fu, Y. Cai, Q. Sun, and B. Zhang, IEEE Trans. Electron Devices **63**, 731 (2016).
[23] X.-F. Zheng, S.-S. Dong, P. Ji, C. Wang, Y.-L. He, L. Lv, X.-H. Ma, and Y. Hao, Appl. Phys. Lett. **112**, 233504 (2018).
[24] D. W. Jenkins, J. D. Dow, and M. Tsai, J. Appl. Phys. **72**, 4130 (1992).
[25] Y. He, P. Li, C. Wang, X. Li, S. Zhao, M. Mi, J. Pei, J. Zhang, X. Ma, and Y. Hao, Appl. Phys. Lett. **107**, 063501 (2015).
[26] G. Wenping, C. Chi, D. Huantao, H. Yue, Z. Jincheng, W. Chong, F. Qian, and M. Xiaohua, J. Semicond. **30**, 044002 (2009).

Published under an exclusive license by AIP Publishing